REPORT DOCUMENTATION PAGE

Form Approved OMB NO. 0704-0188

1. REPORT DATE (DD-MM-YYYY)	2. REPORT TYPE	3. DATES COVERED (From - To)
	New Reprint	-

4. TITLE AND SUBTITLE

Sulfur dioxide and nitrogen dioxide adsorption on zinc oxide and zirconium hydroxide nanoparticles and the effect on photoluminescence

5a. CONTRACT NUMBER
W911NF-11-1-0213

5b. GRANT NUMBER

5c. PROGRAM ELEMENT NUMBER
206023

6. AUTHORS

Jisun Im, Gregory W. Peterson, James E. Whitten, Jagdeep Singh, Anupama Mukherjee, Sandip K. Sengupta

5d. PROJECT NUMBER

5e. TASK NUMBER

5f. WORK UNIT NUMBER

7. PERFORMING ORGANIZATION NAMES AND ADDRESSES

University of Massachusetts - Lowell
University of Massachusetts Lowell
Office of Research Administration
Lowell, MA 01854 -3629

8. PERFORMING ORGANIZATION REPORT NUMBER

9. SPONSORING/MONITORING AGENCY NAME(S) AND ADDRESS(ES)

U.S. Army Research Office
P.O. Box 12211
Research Triangle Park, NC 27709-2211

10. SPONSOR/MONITOR'S ACRONYM(S)
ARO

11. SPONSOR/MONITOR'S REPORT NUMBER(S)
59848-CH.1

12. DISTRIBUTION AVAILIBILITY STATEMENT

Approved for public release; distribution is unlimited.

13. SUPPLEMENTARY NOTES

The views, opinions and/or findings contained in this report are those of the author(s) and should not contrued as an official Department of the Army position, policy or decision, unless so designated by other documentation.

14. ABSTRACT

Nanoparticulate zinc oxide and micron-size zirconium hydroxide powders have been exposed to sulfur dioxide and nitrogen dioxide by flowing the gases, diluted with nitrogen, over powder samples. X-ray photoelectron spectroscopy (XPS), Raman spectroscopy, and thermal gravimetric analyses (TGA) indicate strongly bound, chemisorbed SO3 and NO3 surface species. Two pre-treatments of the nanoparticulate ZnO samples prior to gas exposure have been investigated: 1) drying overnight in a vacuum oven and 2) hydrating the samples by placing

15. SUBJECT TERMS

Metal oxide, photoelectron spectroscopy, photoluminescence, sensor

16. SECURITY CLASSIFICATION OF:			17. LIMITATION OF ABSTRACT	15. NUMBER OF PAGES	19a. NAME OF RESPONSIBLE PERSON
a. REPORT	b. ABSTRACT	c. THIS PAGE			James Whitten
UU	UU	UU	UU		19b. TELEPHONE NUMBER: 978-934-3666

Report Title

Sulfur dioxide and nitrogen dioxide adsorption on zinc oxide and zirconium hydroxide nanoparticles and the effect on photoluminescence

ABSTRACT

Nanoparticulate zinc oxide and micron-size zirconium hydroxide powders have been exposed to sulfur dioxide and nitrogen dioxide by flowing the gases, diluted with nitrogen, over powder samples. X-ray photoelectron spectroscopy (XPS), Raman spectroscopy, and thermal gravimetric analyses (TGA) indicate strongly bound, chemisorbed SO3 and NO3 surface species. Two pre-treatments of the nanoparticulate ZnO samples prior to gas exposure have been investigated: 1) drying overnight in a vacuum oven and 2) hydrating the samples by placing them overnight in water-saturated air. A dramatic difference in reactivity of ZnO is observed, with approximately two-fold and ten-fold greater uptake of NO2 and SO2, respectively, measured by XPS for the hydrated samples relative to the dried ones. Transmission electron microscopy (TEM) demonstrates that the greater uptake arises from a morphology change in the case of the hydrated samples, and it is postulated that this is due to dissolution of the gases in physisorbed water, which leads to acids that partially erode the ZnO and lead to greater surface area. For zirconium hydroxide, no morphology change is observed for hydrated samples, and SO4 (ads), in addition to SO3 (ads), is indicated by XPS. ZnO and Zr(OH)4 both exhibit photoluminescence (PL) spectra, with peak intensities that change dramatically due to hydration and subsequent exposure to SO2 and NO2 gases. Dosing of the powders with these gases effectively reverts the PL spectra to those corresponding to less hydration.

REPORT DOCUMENTATION PAGE (SF298)
(Continuation Sheet)

Continuation for Block 13

ARO Report Number 59848.1-CH
Sulfur dioxide and nitrogen dioxide adsorption o ...

Block 13: Supplementary Note

Approved for public release; distribution is unlimited.

Applied Surface Science 258 (2012) 5778–5785

Contents lists available at SciVerse ScienceDirect

Applied Surface Science

journal homepage: www.elsevier.com/locate/apsusc

Sulfur dioxide and nitrogen dioxide adsorption on zinc oxide and zirconium hydroxide nanoparticles and the effect on photoluminescence

Jagdeep Singh [a], Anupama Mukherjee [a], Sandip K. Sengupta [a], Jisun Im [a], Gregory W. Peterson [b], James E. Whitten [a,*]

[a] Department of Chemistry, University of Massachusetts Lowell, Lowell, MA 01854, United States
[b] U.S. Army Edgewood Chemical Biological Center, Aberdeen Proving Ground, MD 21010, United States

ARTICLE INFO

Article history:
Received 22 September 2011
Received in revised form
25 December 2011
Accepted 20 February 2012
Available online 24 February 2012

Keywords:
Metal oxide
Photoelectron spectroscopy
Photoluminescence
Sensor

ABSTRACT

Nanoparticulate zinc oxide and micron-size zirconium hydroxide powders have been exposed to sulfur dioxide and nitrogen dioxide by flowing the gases, diluted with nitrogen, over powder samples. X-ray photoelectron spectroscopy (XPS), Raman spectroscopy, and thermogravimetric analysis (TGA) indicate strongly bound, chemisorbed SO_3 and NO_3 surface species. Two pre-treatments of the nanoparticulate ZnO samples prior to gas exposure have been investigated: (1) drying overnight in a vacuum oven and (2) hydrating the samples by placing them overnight in water-saturated air. A dramatic difference in reactivity of ZnO is observed, with approximately two-fold and ten-fold greater uptake of NO_2 and SO_2, respectively, measured by XPS for the hydrated samples relative to the dried ones. Transmission electron microscopy (TEM) demonstrates that the greater uptake arises from a morphology change in the case of the hydrated samples. For zirconium hydroxide, no morphology change is observed for hydrated samples, and SO_4 (ads), in addition to SO_3 (ads), is indicated by XPS. ZnO and $Zr(OH)_4$ both exhibit photoluminescence (PL) spectra, with peak intensities that change dramatically due to hydration and subsequent exposure to SO_2 and NO_2 gases. Dosing of the powders with these gases effectively reverts the PL spectra to those corresponding to less hydration.

1. Introduction

Surface reactions of metal oxides and hydroxides are important for various applications such as gas sensing, catalysis and industrial processes involving removal of toxic gases [1–6]. ZnO is one of the most studied metal oxides and has potential for a broad range of optical, electronic and piezoelectric applications [7,8]. Nanoparticulate ZnO has a bimodal photoluminescence (PL) spectrum consisting of an excitonic ultraviolet (UV) emission peak and a visible peak arising from nonradiative transfer of an excited electron from the conduction band to a lower lying electronic state, originating from surface defect states, and subsequent decay from this state to the valence band [9]. Idriss and Barteau [10] investigated the effect of various adsorbates (O_2, CO, H_2, COOH and CH_3OH) on the photoluminescence behavior of ZnO surfaces and concluded that the photoluminescence is sensitive to the nature of the adsorbate. Rodriguez and co-workers [11–13] studied the chemistry of SO_2 and NO_2 on polycrystalline ZnO using photoelectron spectroscopy. Their studies indicate that these molecules chemisorb to the surface by bonding to oxygen sites, forming adsorbed SO_3 and NO_3.

Zirconium hydroxide has been investigated by Peterson et al. [5,6] for its ability to remove sulfur dioxide in respirator applications. The removal capacity was found to be high relative to impregnated activated carbon, and filtration breakthrough curves showed that SO_2 is strongly bound to $Zr(OH)_4$. X-ray photoelectron spectroscopy (XPS) revealed the formation of zirconia sulfite [$Zr(SO_3)_2$], and the data suggested that a small fraction (ca. 10%) of the surface hydroxyl groups are replaced by SO_2.

In the present study, we have examined differences in reactivity of dried and hydrated ZnO nanoparticles to SO_2 and NO_2 gases. In addition to establishing that SO_3 (ads) and NO_3 (ads) are formed on the surface, X-ray photoelectron spectroscopy experiments demonstrate that physisorbed water dramatically affects the amount of chemisorption. Adsorption of SO_3 and NO_3 are confirmed by Raman spectroscopy. Electron microscopy shows that the morphology of the hydrated nanoparticles changes upon gas exposure, with greater adsorption due to degradation of the particles and greater surface area. It is further shown that the photoluminescence spectra of the nanoparticulate ZnO change due to hydration and to gas exposure. In the case of $Zr(OH)_4$, SO_3 and NO_3 species also form on the surface. However, no change in morphology is observed related to the degree of hydration. $Zr(OH)_4$ exhibits strong

* Corresponding author. Tel.: +1 978 934 3666.
E-mail address: James_Whitten@uml.edu (J.E. Whitten).

0169-4332/$ – see front matter © 2012 Elsevier B.V. All rights reserved.
doi:10.1016/j.apsusc.2012.02.093

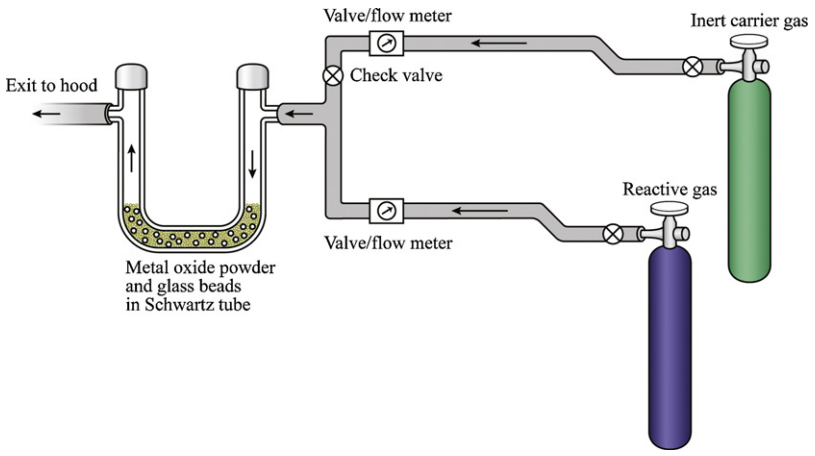

Fig. 1. Experimental setup used to expose metal oxide and metal hydroxide powders to sulfur dioxide and nitrogen dioxide gases.

PL which is affected by the degree of hydration and SO_3 and NO_3 chemisorption. The origins of the changes in the PL spectra are discussed.

2. Experimental

Nanoparticulate ZnO, with an average particle size of 20 nm, was purchased from NanoAmor (stock no. 5810HT). To investigate the effect of physisorbed water on reactivity, zinc oxide was either dried overnight in a vacuum oven at 200 °C or stored overnight in a vessel filled with water-saturated air. $Zr(OH)_4$ granules, with a mean size of 7 μm, were prepared as described in ref. [5] using powder purchased from Magnesium Elektron, Inc. (product X20631). The granules were then either used directly (denoted "as-received") or exposed to water-saturated air, as in the case of ZnO. Samples exposed to water-saturated air overnight are referred to as "hydrated".

Unless otherwise specified, sulfur dioxide and nitrogen dioxide exposures were performed using the setup shown in Fig. 1. Approximately 1 g of the nanoparticles was placed in the U-shaped Schwartz drying tube, with glass beads added to increase the surface area and facilitate enhanced contact with the flowing gas. To remove air prior to gas exposure, pure nitrogen was passed through the tube for 10 min at a flow rate of 150 ml/min. The reactive gas was then added at a flow rate of 30 ml/min, such that a reactive-to-inert gas ratio (by volume) of 1:5 was used. The nanoparticles were exposed to the gas mixture for a total of 20 min. They were then purged briefly with pure nitrogen and stored in a capped bottle for analysis.

Vacuum compatible, double-sided adhesive carbon tape was used to attach nanoparticle samples on stubs for transfer into the VG ESCALAB MKII X-ray photoelectron spectroscopy instrument equipped with an Mg Kα X-ray source ($h\upsilon$ = 1253.6 eV). Photoelectrons were detected using a pass energy of 20 eV and a take-off angle of 90°, defined as the angle between the surface plane and the entrance of the focusing lens of the analyzer. XPS spectra were corrected for surface charging, which occurs due to incomplete compensation of ejected electrons, by shifting all of the spectral regions by the energy necessary to align the Zn $2p_{3/2}$ peak to 1021.7 eV, the known binding energy of zinc oxide [14]. For zirconium hydroxide, the observed binding energy for the Zr $3d_{5/2}$ peak was 182.4 eV. This is in excellent agreement with the expected value for ZrO_2, which is essentially identical to the Zr $3d_{5/2}$ binding energy for $Zr(OH)_4$, and no corrections for charging were necessary. Atomic ratios for elements in a particular sample have been calculated by integrating the areas under the XPS peaks of interest (e.g., S 2p and Zn $2p_{3/2}$), dividing the areas by the appropriate sensitivity factors, and ratio-ing the values. Direct comparison of intensities and areas for different samples is not possible due to sample-to-sample variation in charging and sample angle. Therefore, intensities of multiple XPS spectra shown in a particular figure should not be directly compared.

Photoluminescence spectra were acquired using a FluoroMax-3 fluorescence spectrometer (Horiba Jobin Yvon, Inc.) equipped with a solid sample holder accessory. The angle of incidence was optimized for the best signal to noise ratio but held constant for each group of samples. Optical filters were placed in both the excitation and emission paths in order to suppress stray light, to further monochromatize the exciting light and to prevent scattered excitation light from entering the detection system. In the case of ZnO, Hoya U340 and Newport CGA-345 filters, and for $Zr(OH)_4$ PL measurements, Hoya U340 and Schott GG385 filters, were used in the excitation and emission paths, respectively. The excitation wavelength for the ZnO and $Zr(OH)_4$ samples was 325 nm. Thermogravimetric analysis (TGA) under nitrogen atmosphere was performed using a DuPont TGA 2950 instrument at a heating rate

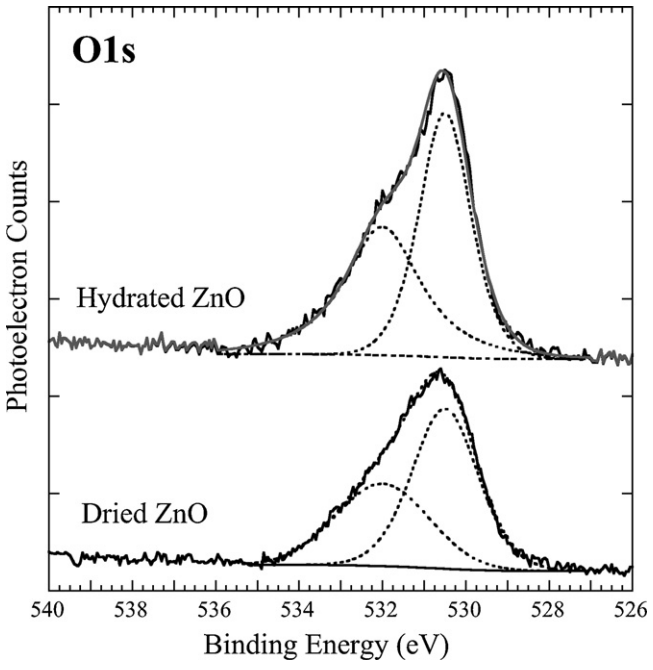

Fig. 2. Mg Kα XPS of the O 1s region of dried and hydrated zinc oxide nanospheres.

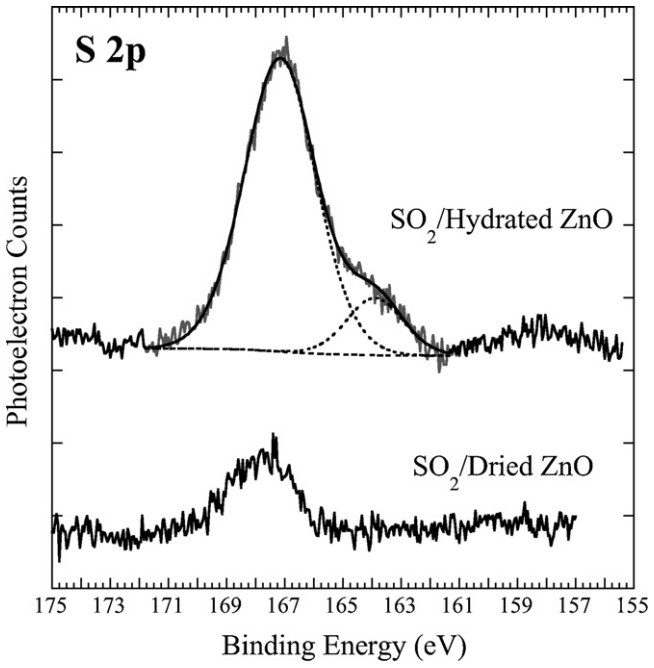

Fig. 3. Mg Kα XPS of the S 2p region of dried and hydrated zinc oxide nanospheres after exposure to sulfur dioxide.

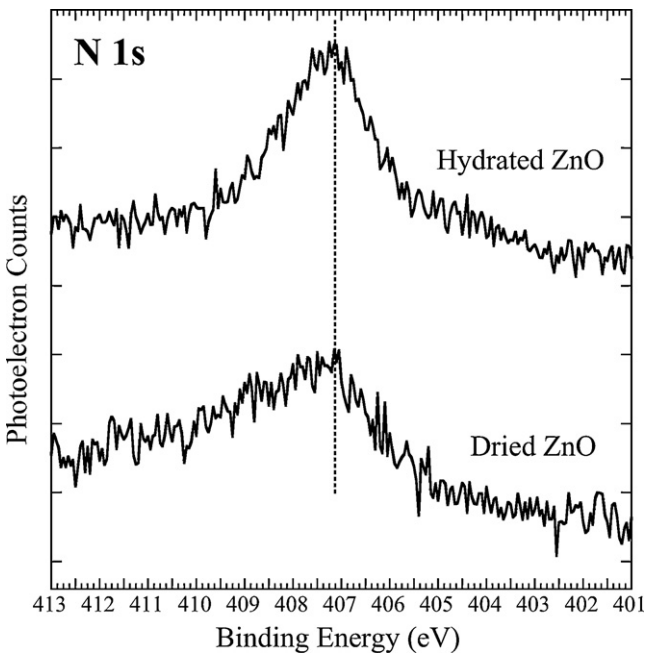

Fig. 4. Mg Kα XPS of the N 1s region of dried and hydrated zinc oxide nanospheres after exposure to nitrogen dioxide.

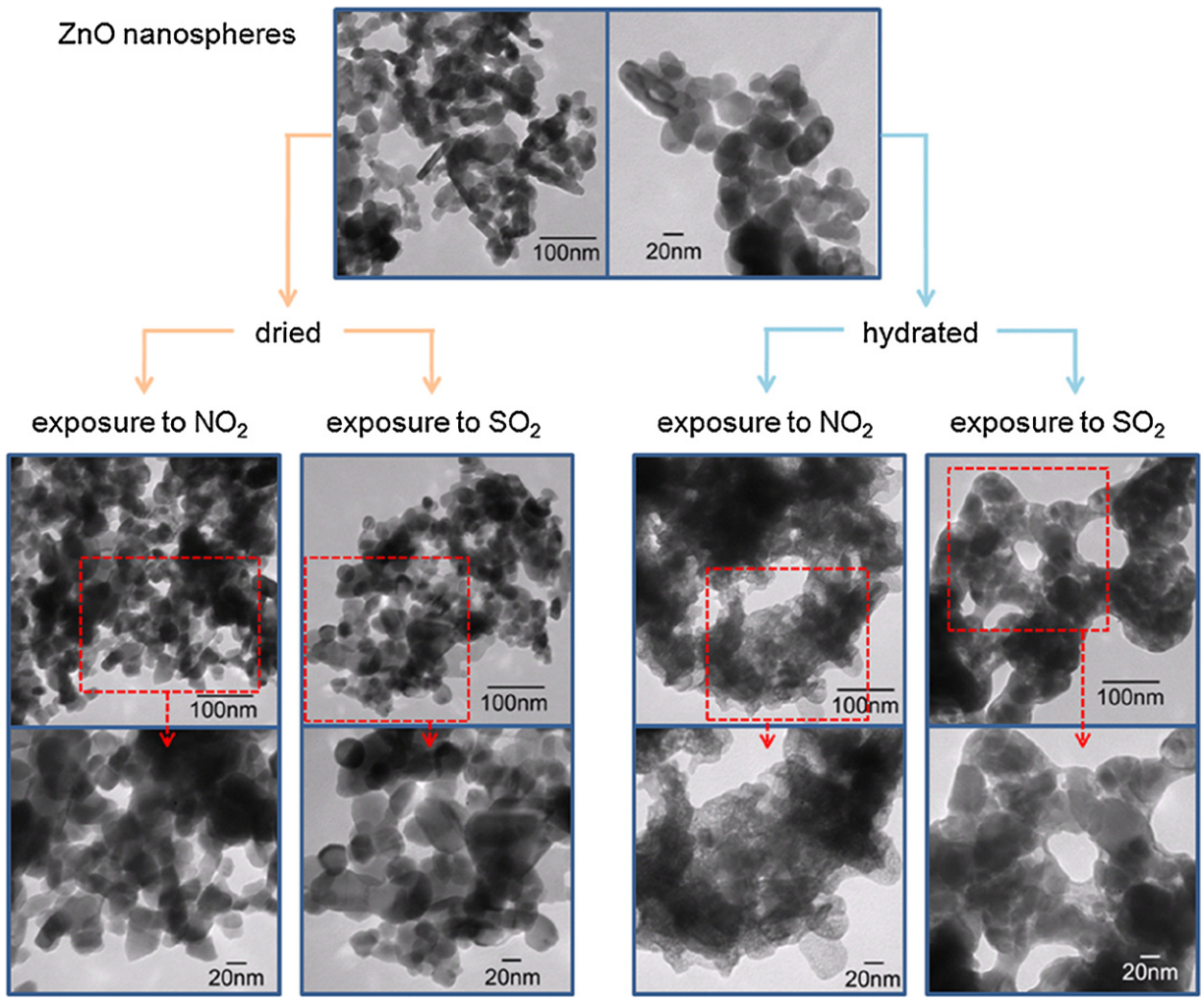

Fig. 5. TEM images of dried and hydrated ZnO nanospheres before and after exposure to nitrogen dioxide and sulfur dioxide. All samples are shown at two different magnifications, with the untreated sample shown at lower magnification on the top left and at higher magnification on the top right.

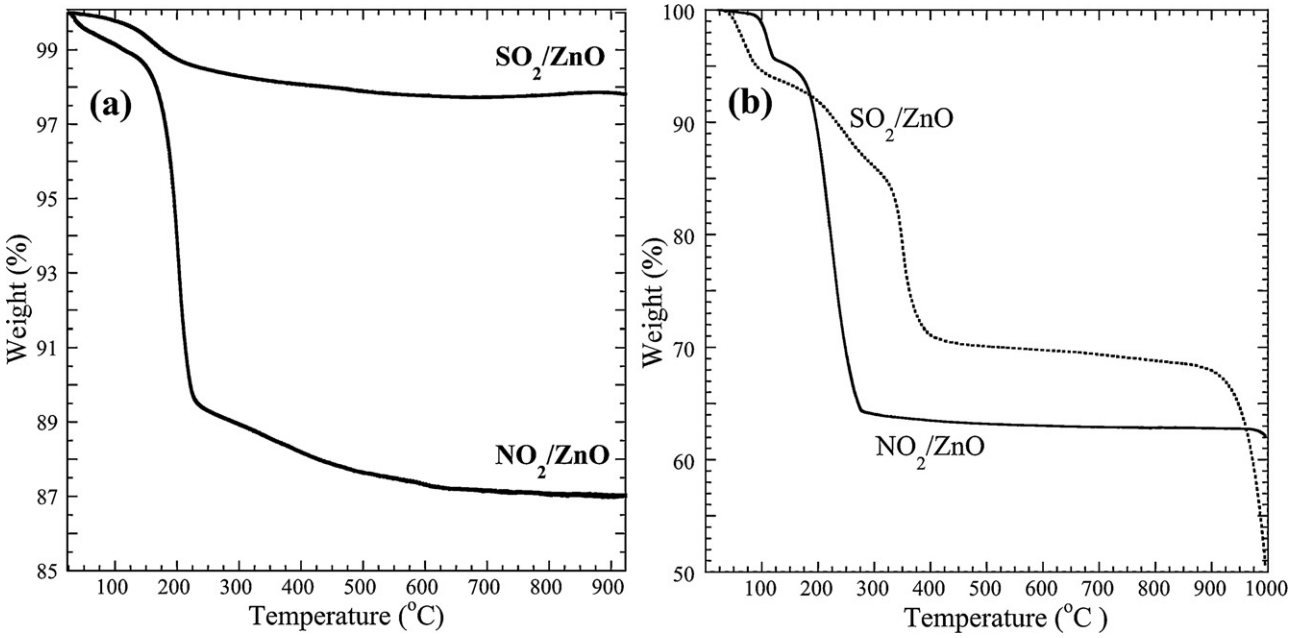

Fig. 6. Thermal gravimetric analysis of (a) SO_2- and NO_2-exposed dried zinc oxide and (b) SO_2- and NO_2-exposed hydrated zinc oxide.

of 10 °C/min. Transmission electron microscopy (TEM) experiments were performed using a Philips EM 400t microscope and an accelerating voltage of 100 kV. Raman spectroscopy measurements were carried out with a Bruker Senterra microscope system. The excitation wavelength was 532 nm at a power of 20 mW in a spot size of ca. 5 μm.

3. Results and discussion

3.1. Zinc oxide

Fig. 2 displays O 1s XPS spectra of dried and hydrated nanoparticulate ZnO. Peak fitting was performed with a Shirley-type background and 35% Lorentzian/65% Gaussian components. Two components are identified at 530.5 and 532.0 eV. These correspond to oxygen present in bulk ZnO and in hydroxyl groups and water bonded to the surface of the ZnO nanoparticles, respectively. Integration of the peaks corresponding to the two components yields O(OH)/and O(bulk) ratios for the dried and hydrated ZnO NPs of 0.69 and 0.80, respectively, consistent with higher water content in the latter sample.

S 2p XPS spectra of sulfur dioxide-exposed hydrated and dried nanoparticulate ZnO samples are shown in Fig. 3. For reference, the S $2p_{3/2}$ peak binding energies for SO_2, SO_3 and SO_4 adsorbed on ZnO are ca. 165.6, 166.8, and 168.0 eV, respectively [12]. The strong sulfur peaks observed in the range of 167.0–167.5 eV are

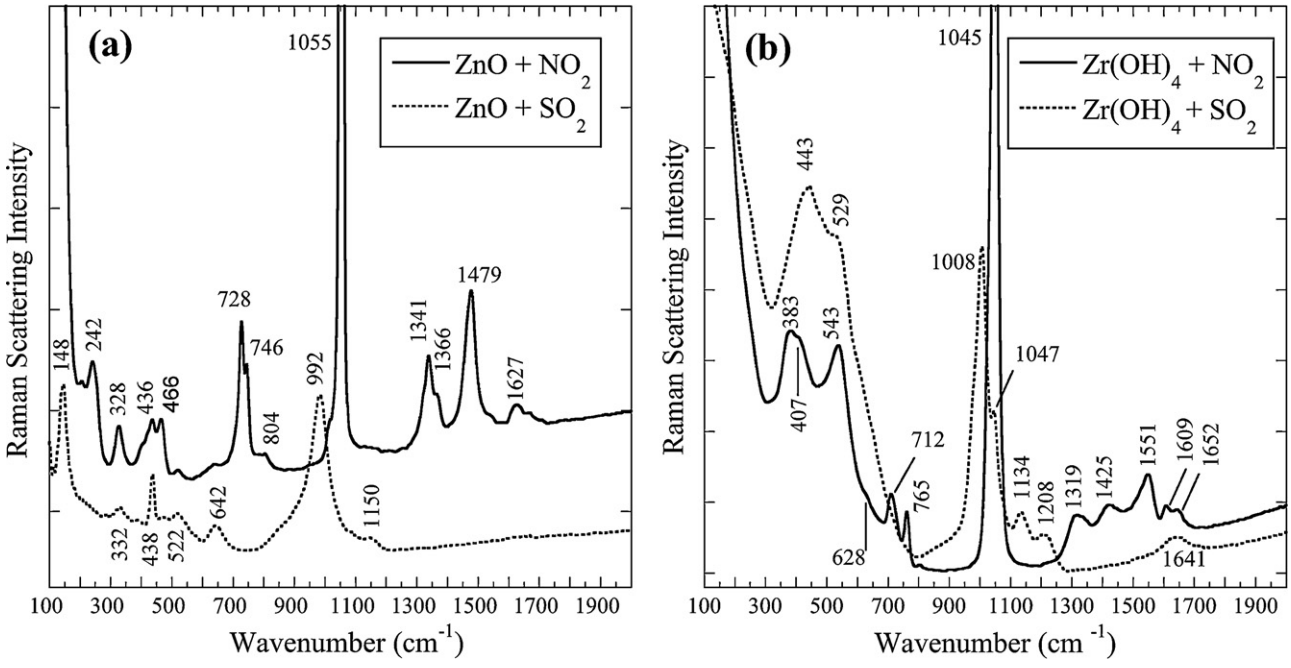

Fig. 7. Raman spectra of (a) hydrated ZnO nanospheres exposed to sulfur dioxide and nitrogen dioxide and (b) $Zr(OH)_4$ powder exposed to these gases. The laser wavelength was 532 nm.

consistent with the molecule being adsorbed as SO_3 and possibly SO_4, via adsorption on O sites. Interestingly, in the case of the hydrated ZnO sample, a small amount of SO_2 is also present, indicative of some chemisorption on Zn sites. The S/Zn ratio following exposure of dried and hydrated ZnO samples to sulfur dioxide is 0.11 and 1.3, respectively.

Fig. 4 displays corresponding N 1s XPS data for nitrogen dioxide-exposed dried and hydrated ZnO. The binding energy at 407.1 eV is consistent with NO_3 adsorption, as observed by Rodriguez et al. [12] at 406.9 eV for ultrahigh vacuum-dosing of polycrystalline and single crystal zinc oxide with nitrogen dioxide. For reference, adsorbed NO_2 has a peak N 1s binding energy of 403.6 eV [12]. The high binding energy shoulder at ca. 409 eV of the dried sample likely originates from NO_3 bonded on more than one type of site compared to the hydrated sample; in other words, the bonding is less homogeneous for the dried sample. The reason for this difference is not clear. The N/Zn ratio following exposure of dried and hydrated ZnO samples to nitrogen dioxide is 0.2 and 0.4, respectively.

These results indicate that hydration of the ZnO prior to SO_2 and NO_2 exposure causes an increased uptake relative to dried ZnO. Fig. 5 shows transmission electron microscope images of dried and hydrated ZnO nanoparticles before and after exposure to the two gases. The images clearly demonstrate that a morphology change occurs upon exposure of the hydrated particles to the gases; this does not occur for the dried samples. For the hydrated samples, exposure to the gases leads to erosion and partial dissolution with a concomitant increase in surface area. This is, at least partially, responsible for the greater gas uptake relative to the dried samples. One may speculate that the mechanism for this morphology change is that physisorbed water dissolves NO_2 and SO_3, with the latter removed from the surface of the ZnO particles, and forms nitric acid and sulfuric acid, respectively. ZnO is known to be dissolved by acids [18], which would be consistent with the TEM images in the figure.

Fig. 6a and b shows TGA data for dried and hydrated ZnO samples, respectively, after exposure to SO_2 and NO_2. While a small amount of desorption occurs below 100 °C, in all cases, the majority of the weight loss occurs above this temperature. In the case of the SO_2-dosed sample, the greatest decrease in mass occurs at ca. 175 °C. Rodriguez et al. [12] observed the disappearance of the X-ray absorption near edge spectroscopy peak arising from SO_3 upon heating to 50–100 °C. A small signal persisted to temperatures as high as 350 °C and was postulated by the authors possibly to be due to adsorbed SO_4. For the NO_2 data in Fig. 6, the corresponding temperature is ca. 200 °C. As discussed previously, XPS indicates that the adsorbed species is NO_3. Our results are consistent with ref. [12], which found that NO_3 desorbed from ZnO(0 0 0 1) at ca. 230 °C. In the case of dried ZnO (Fig. 6a), the larger weight loss for the NO_2-exposed sample is due to the greater amount of adsorption compared to SO_2.

Fig. 7a shows Raman spectroscopy measurements of reactive gas-exposed hydrated ZnO. In the case of the NO_2-exposed samples, bands above 650 cm^{-1} are assigned to intramolecular adsorbate vibrations, consistent with the known spectra of inorganic nitrates [15]. Bands below 650 cm^{-1} are attributed to metal–oxygen vibrations. The band containing the 728 and 746 cm^{-1} peaks is due to O—N—O scissoring, and the very strong peak at 1055 cm^{-1} corresponds to O—N—O symmetric stretches. The peaks in the range of 1300–1500 cm^{-1} are assignable to N—O asymmetric stretches [16]. For SO_2-exposed ZnO, peaks at 148, 332, 438, 522, 642, 992 and 1150 cm^{-1} are consistent with adsorbed SO_3 and similar to those in sodium sulfite, which displays bands at 496, 635, 980, 1005, and 1135 cm^{-1} [17]. The peaks at 148 and 332 cm^{-1} are, therefore, assigned to Zn—O—S stretches.

Fig. 8a shows photoluminescence spectra of dried and hydrated ZnO nanoparticle samples, which consist of two main features: a

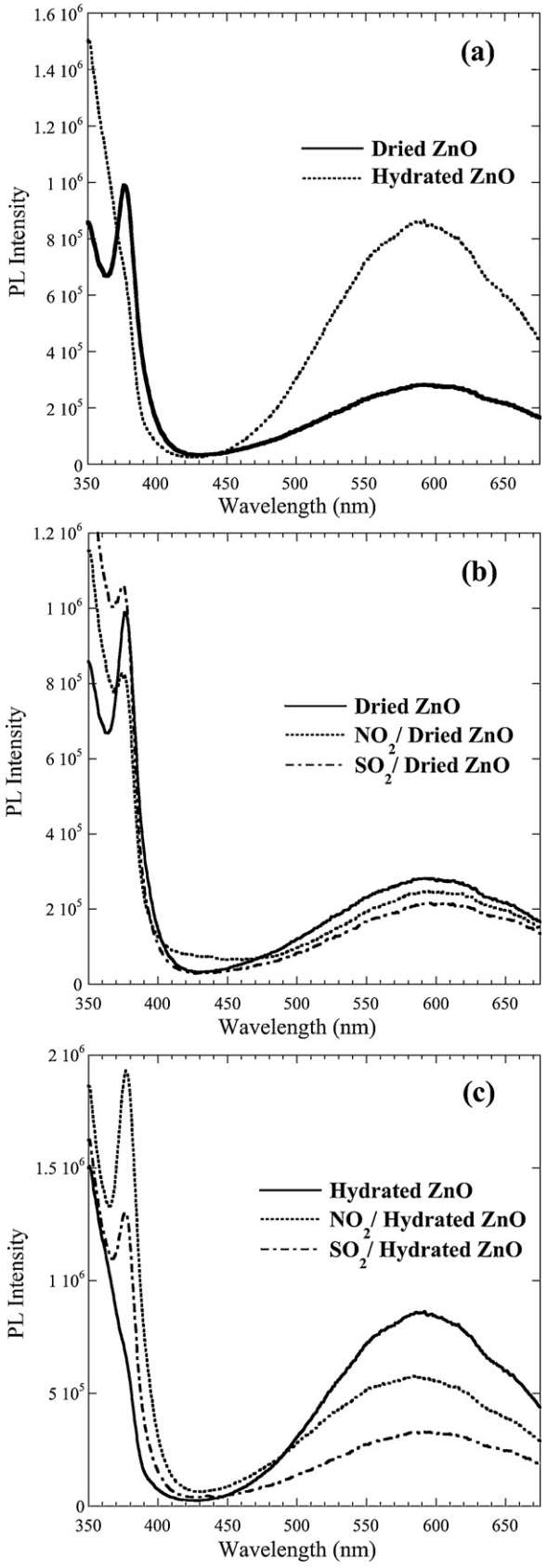

Fig. 8. Photoluminescence emission spectra of (a) dried and hydrated ZnO; (b) dried ZnO after exposure to nitrogen dioxide and sulfur dioxide; and (c) hydrated ZnO after exposure to nitrogen dioxide and sulfur dioxide. The excitation wavelength was 325 nm.

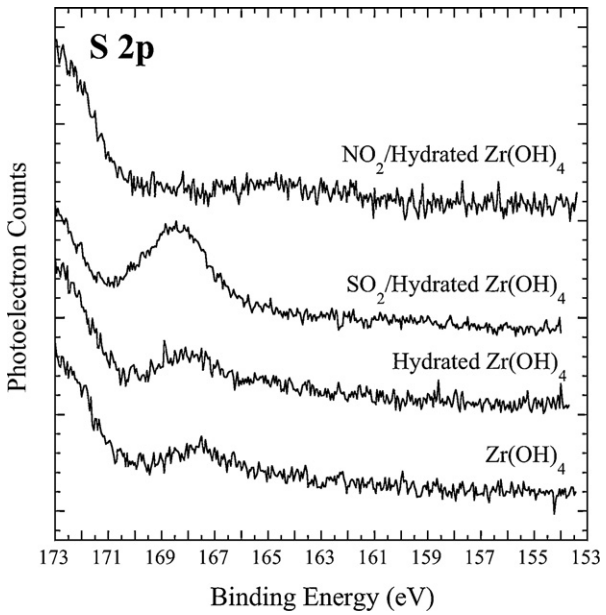

Fig. 9. Mg Kα XPS of the S 2p region of as-received zirconium hydroxide, hydrated zirconium hydroxide, and hydrated zirconium hydroxide after exposure to sulfur dioxide and nitrogen dioxide.

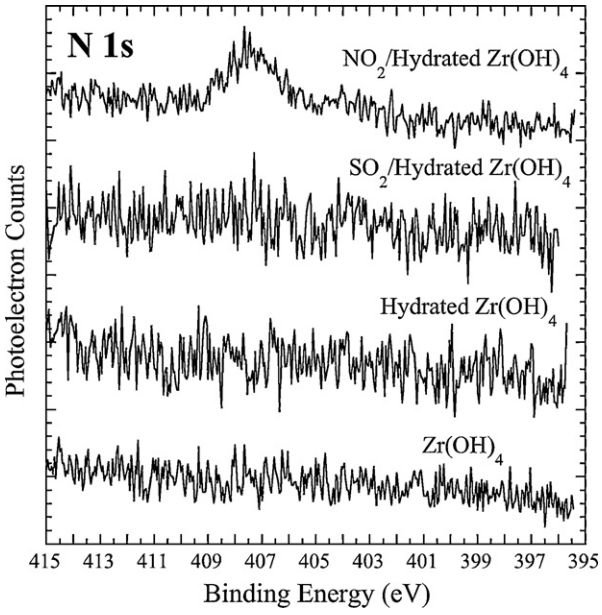

Fig. 10. Mg Kα XPS of the N 1s region of as-received zirconium hydroxide, hydrated zirconium hydroxide, and hydrated zirconium hydroxide after exposure to sulfur dioxide and nitrogen dioxide.

narrow UV emission band peaked at 380 nm and a broad visible band peaked at 590 nm. The UV peak originates from excitonic recombination, and the visible emission is believed to be due to recombination of an electron in or near the conduction band with a hole at a defect site such as an oxygen vacancy [9]. The presence of physisorbed water causes a decrease in the intensity of the UV peak and an increase in that of the visible peak, with the water apparently increasing the lifetime of the defect-driven emission path. The two radiative emission paths are in competition, and an increase in the visible emission path occurs at the expense of the excitonic one. As shown in Fig. 8b, exposure of dried nanoparticulate ZnO to NO_2 and SO_2 causes a decrease and an increase, respectively, in the UV emission peak intensity. In both cases, the intensity of the visible peak decreases slightly. While the changes are relatively minor for the dried samples, they are dramatic for the hydrated ones, consistent with the morphology changes discussed previously. As illustrated in Fig. 8c, exposure to the gases causes reappearance of the UV emission peak, which was lost from water exposure, and a decrease in the visible emission peak.

Norberg and Gamelin [19] studied the effect of adsorbates on the PL of colloidal ZnO nanocrystals. These authors concluded that the visible emission arising from trap states is directly correlated with surface hydroxide concentration. Furthermore, the intensity of the UV (excitonic) emission peak was found to be inversely proportional to the number of surface defects. In the present study, the most likely explanation of the changes induced by gas dosing of hydrated ZnO is as follows. (1) Hydration causes an increase in the surface concentration of hydroxide groups and trap states,

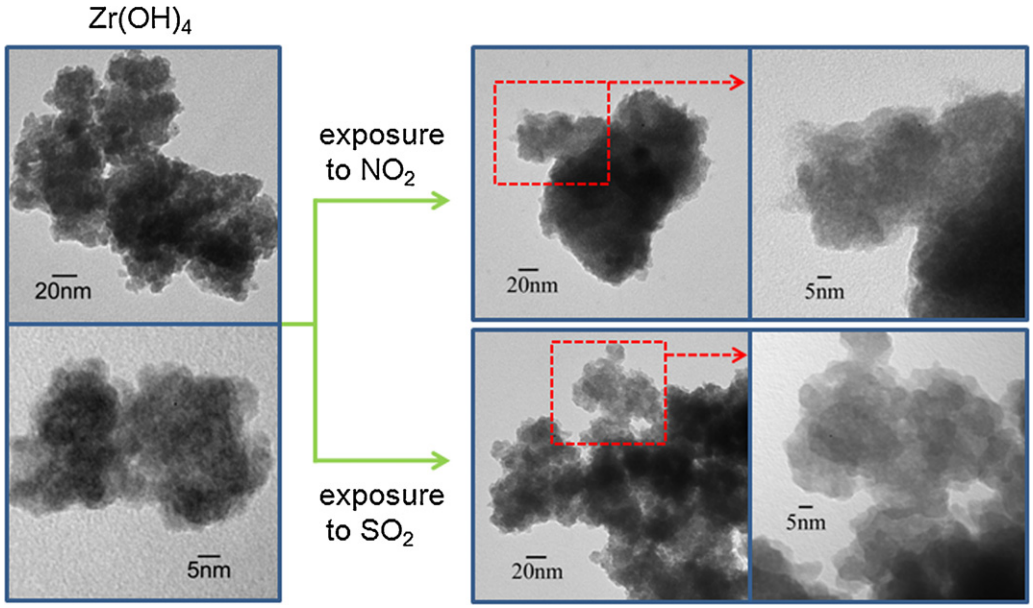

Fig. 11. TEM images of hydrated $Zr(OH)_4$ after exposure to nitrogen dioxide and sulfur dioxide. All samples are shown at two different magnifications, with the untreated sample shown at lower magnification on the top left and at higher magnification on the bottom left.

leading to an increase in the visible emission peak and a decrease in the UV one. (2) Dosing with SO_2 or NO_2 leads to displacement of a fraction of the adsorbed hydroxide groups and, more importantly, to a reduction in the number of defects. This leads to reversion of the spectrum to essentially the same spectrum obtained for ZnO prior to hydration.

3.2. Zirconium hydroxide

Figs. 9 and 10 display S 2p and N 1s XPS spectra, respectively, of nanoparticulate $Zr(OH)_4$ exposed to SO_2 and NO_2 gases. The binding energies of the S 2p and N 1s peaks after exposure are 168.4 and 407.3 eV, respectively. Some sulfur contamination is observed even prior to SO_2 exposure. Peterson et al. [5,6] studied SO_2 adsorption on similar $Zr(OH)_4$ samples and measured an S 2p peak binding energy of 167.4 ± 0.2 eV; they identified SO_3 as the dominant surface species. Our higher binding energy and broad S 2p peak suggest that surface SO_3 and SO_4 species are present. For NO_2 exposure, the N 1s peak binding energy is ca. 407.4 eV. While the identity of the metal (Zr vs. Zn) can cause some minor differences, the S 2p and N 1s binding energies for $Zr(OH)_4$ following gas exposure are generally in agreement with those for ZnO, indicating that SO_3 and NO_3 are the adsorbed species on both ZnO and $Zr(OH)_4$ powders. Some SO_4 (ads) is also indicated in the case of $Zr(OH)_4$.

Raman spectra of NO_2- and SO_2-exposed hydrated $Zr(OH)_4$ are included as Fig. 7b. For reference, gels of $Zr(OH)_2(NO_3)_2$ exhibit Zr—O stretches at 375, 430, 545, and 630 cm^{-1} [20]. In the case of the NO_2-dosed sample, the bands at 712 and 765 cm^{-1} arise from O—N—O scissoring. The strong peak at 1045 cm^{-1} corresponds to the O—N—O symmetric stretches. The peaks in the range of 1300–1500 cm^{-1} are assignable to the N—O asymmetric stretches. For the SO_2-exposed $Zr(OH)_4$, peaks are observed at 443, 529, 1008, 1134, 1208, and 1641 cm^{-1}. These energies are similar to those for the ZnO sample, except for the 1208 and 1641 cm^{-1} peaks. The former may be due to the SO_4 asymmetric (ν_2) stretching mode. The 1641 cm^{-1} peak is likely due to a water-bending mode. Because many of the sulfite and sulfate Raman peaks are similar in energy, most of the sulfate peaks are likely buried within the predominant sulfite spectrum for the $Zr(OH)_4$ sample.

TEM images of $Zr(OH)_4$ before and after SO_2 and NO_2 exposure are displayed in Fig. 11. This material appears as amorphous agglomerates and does not exhibit well-defined particles, as in the case of the ZnO sample (Fig. 5). The lighter, less dense regions of the sample are consistent with the previously reported porosity of this material [5,6]. As shown in the figure, no significant differences are observed following gas exposure.

The photoluminescence of $Zr(OH)_4$ has not been previously investigated, and this represents the first study of how it is affected by adsorption. As shown in Fig. 12a, particulate $Zr(OH)_4$ exhibits a spectrum consisting of an apparent UV emission peak at ca. 372 nm and a visible emission peak at 420 nm, respectively. The "UV emission peak" actually is not due to photoluminescence but mainly to Raman scattering from physisorbed water, as confirmed by experiments using different excitation wavelengths; these experiments show that this "emission" peak shifts by the same amount as the excitation peak. There is also some contribution from Rayleigh scattering in this peak. Hydration of as-received $Zr(OH)_4$ results in an increase in the UV-to-visible peak ratio and a small blue shift in the visible peak (from 425 nm to 420 nm), consistent with additional physisorbed water causing greater Raman scattering. Fig. 12b and c demonstrates the effect of SO_2 and NO_2 exposure. In both cases, the pair of emission peaks decreases in intensity, with the visible peak shifting slightly to longer wavelength (from 420 nm to 426 and 430 nm, respectively, for SO_2 and NO_2 exposure). The decrease in PL intensities and the red shift in the visible emission peak suggest that SO_3 and NO_3 adsorption occurs at the expense of adsorbed hydroxyl

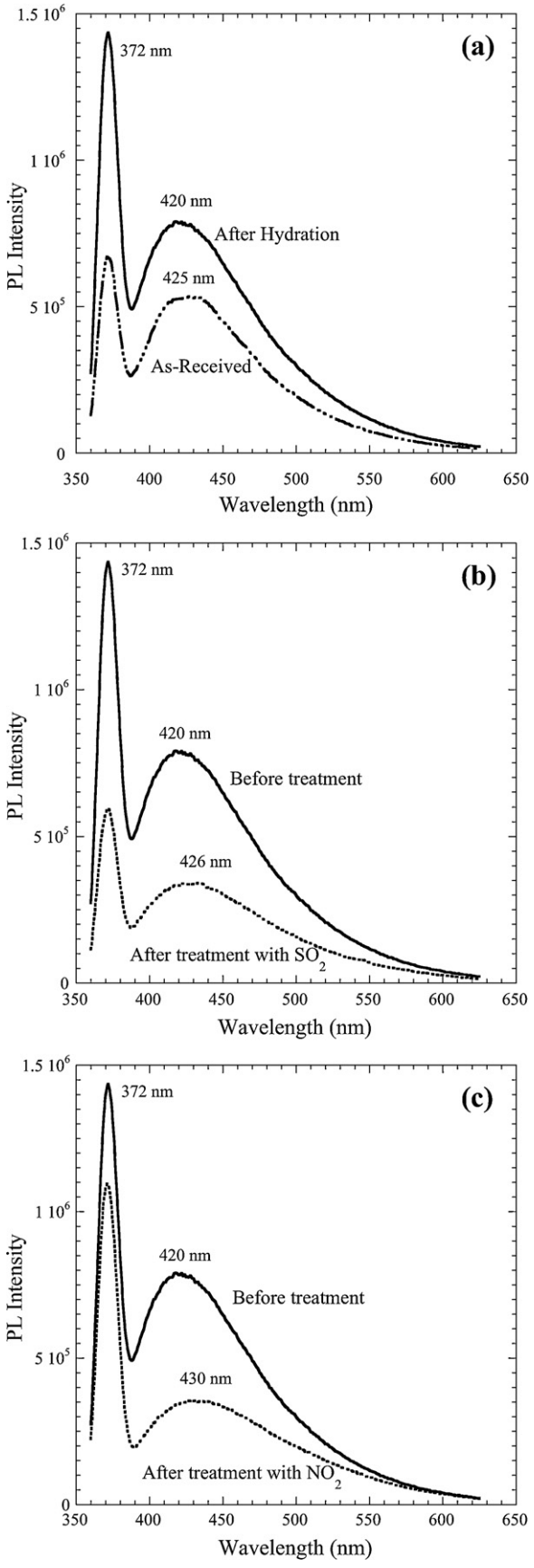

Fig. 12. Photoluminescence emission spectra of (a) as-received and hydrated zirconium hydroxide and; (b) hydrated zirconium hydroxide before and after exposure to SO_2; hydrated zirconium hydroxide before and after exposure to NO_2.

groups. This manifests itself in the PL spectrum in that hydration (i.e., saturation with hydroxyl groups) is effectively undone by SO_2 and NO_2 exposure. This supports the conclusion in refs. [5,6] that SO_2 exposure results in dehydroxylation of the surface.

4. Conclusions

XPS and Raman spectroscopy confirm that exposure of ZnO and $Zr(OH)_4$ powders to SO_2 and NO_2 results in SO_3 and NO_3 chemisorption. Exposure of ZnO to water-saturated air prior to reactive gas dosing enhances its adsorption capacity, with the increased uptake arising from a change in morphology and higher surface area. The effect is most pronounced for SO_2, in which a ten-fold increase in adsorption occurs due to hydration. The change in morphology occurs due to physisorbed water, which dissolves NO_2 and adsorbed SO_3; the acids subsequently erode the ZnO. The effect of varying the water content of $Zr(OH)_4$ was not extensively studied. However, no morphology change was observed for hydrated samples following reactive gas exposure.

ZnO and $Zr(OH)_4$ powders are photoluminescent, both exhibiting UV and visible emission peaks, although the $Zr(OH)_4$ emission peak is due to Raman scattering from physisorbed water. Hydration has contrasting effects on these samples. In the case of ZnO, it results in a decrease in the UV and an increase in the visible emission peaks. Exposure to the reactive gases effectively undoes the effects of water exposure, with reversion of the PL spectrum to essentially that of dried ZnO. For $Zr(OH)_4$, hydration causes an increase in the intensities of both the UV (Raman) and visible peaks and a slight blue shift in the latter. SO_2 and NO_2 exposure cause the intensities of both peaks to decrease and the visible one to red-shift. For both ZnO and $Zr(OH)_4$, these data suggest that SO_3 and NO_3 chemisorption replace some of the adsorbed hydroxyl groups. A detailed study is underway to investigate the role that adsorbed water and SO_2 and NO_2 have on the photoluminescence spectrum of $Zr(OH)_4$.

Acknowledgments

The authors acknowledge support of the Army Research Office. This work was conducted under Defense Threat Reduction Agency, Project no. BA07PR0105.

References

[1] V.E. Henrich, P.A. Cox, The Surface Science of Metal Oxides, Cambridge University Press, 1994.
[2] J.A. Rodriguez, D. Stacchiola, Catalysis and the nature of mixed-metal oxides at the nanometer level: special properties of MOx/TiO_2(1 1 0) {M = V, W, Ce} surfaces, Phys. Chem. Chem. Phys. 12 (2010) 9557–9565.
[3] G. Ertl, H.-J. Freund, Catalysis and surface science, Phys. Today 52 (1999) 32–38.
[4] J.A. Rodriguez, M. Fernández-Garcia, Synthesis, Properties, and Applications of Oxide Nanomaterials, John Wiley & Sons, 2007.
[5] G.W. Peterson, C. Karwacki, W.B. Feaver, J.A. Rossin, Zirconium hydroxide as a reactive substrate for the removal of sulfur dioxide, Ind. Eng. Chem. Res. 48 (2009) 1694–1698.
[6] G.W. Peterson, J.A. Rossin, C.J. Karwacki, T.G. Glover, Surface chemistry and morphology of zirconia polymorphs and the influence on sulfur dioxide removal, J. Phys. Chem. C 115 (2011) 9644–9650.
[7] C. Wöll, The chemistry and physics of zinc oxide surfaces, Prog. Surf. Sci. 82 (2007) 55–120.
[8] Ü. Özgür, Ya I. Alivov, C. Liu, A. Teke, M.A. Reshchikov, S. Doğan, V. Avrutin, S.-J. Cho, H. Morkoç, A comprehensive review of ZnO materials and devices, J. Appl. Phys. 98 (2005) 041301–42103.
[9] A. van Dijken, E.A. Meulenkamp, D. Vanmaekelbergh, A. Meijerink, J. Phys. Chem. B 104 (2000) 1715–1723.
[10] H. Idriss, M.A. Barteau, Photoluminescence from zinc oxide powder to probe adsorption and reaction of O_2, CO, H_2, HCOOH, and CH_3OH, J. Phys. Chem. 96 (1992) 3382–3388.
[11] S. Chaturvedi, J.A. Rodriguez, T. Jirsak, J. Hrbek, Surface Chemistry of SO_2 on Zn and ZnO: photoemission and molecular orbital studies, J. Phys. Chem. B 102 (1998) 7033–7043.
[12] J.A. Rodriguez, T. Jirsak, S. Chaturvedi, J. Dvorak, Chemistry of SO_2 and NO_2 on ZnO(0 0 0 1)-Zn and ZnO powders: changes in reactivity with surface structure and composition, J. Mol. Catal. A: Chem. 167 (2001) 47–57.
[13] J.A. Rodriguez, T. Jirsak, J. Dvorak, J.S. Sambasivan, D. Fischer, Reaction of NO_2 with Zn and ZnO: photoemission, XANES, and density functional studies on the formation of NO_3, J. Phys. Chem. B 104 (2000) 319–328.
[14] C.D. Wagner, W.M. Riggs, L.E. Davis, J.F. Moulder, G.E. Muilenberg, Handbook of X-Ray Photoelectron Spectroscopy, PerkinElmer, Eden Prairie, MN, 1979.
[15] S.D. Ross, Inorganic Infrared and Raman Spectra, McGraw Hill, London, 1972.
[16] R. Blanco, S. Wang, J.T. Hynes, Infrared signatures of HNO_3 and NO_3^- at a model aqueous surface: a theoretical study, J. Phys. Chem. A 112 (2008) 9467–9476.
[17] R.L. Frost, E.C. Keefe, Raman spectroscopy of the sulfite-bearing minerals scotlandite, hannebachite and orschallite: implications for the desulfation of soils, J. Raman Spectrosc. 40 (2009) 244–248.
[18] L.A.G. Rodenas, M.A. Blesa, P.J. Morado, Reactivity of metal oxides: thermal and photochemical dissolution of MO and MFe_2O_4 (M = Ni, Co, Zn), J. Solid State Chem. 181 (2008) 2350–2358.
[19] N.S. Norberg, D.R. Gamelin, Influence of surface modification on the luminescence of colloidal ZnO nanocrystals, J. Phys. Chem. B 109 (2005), 20810–10816.
[20] P.D. Southon, J.R. Bartlett, J.L. Woolfrey, B. Ben-Nissan, Formation and characterization of an aqueous zirconium hydroxide colloid, Chem. Mater. 14 (2002) 4313–4319.